ORNL/SPR-2022/2532

BISON Validation to In-situ Cladding Burst Test and High Burnup LOCA Experiments

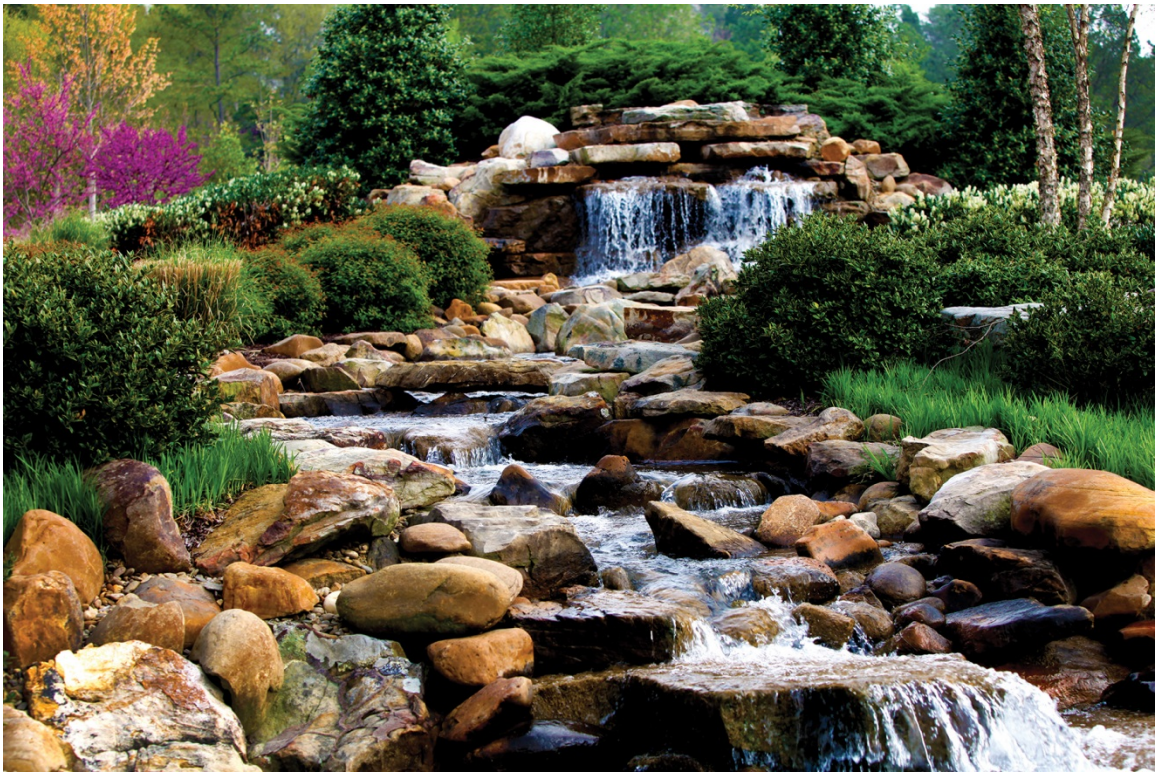

Nathan Capps
Mackenzie Ridley
Samuel Bell
Yong Yan

September 2022

OAK RIDGE National Laboratory

ORNL IS MANAGED BY UT-BATTELLE LLC FOR THE US DEPARTMENT OF ENERGY

ORNL/SPR-2022/2532

Nuclear Energy Advanced Modeling and Simulation

BISON VALIDATION TO IN-SITU CLADDING BURST TEST AND HIGH BURNUP LOCA EXPERIMENTS

Nathan Capps
Mackenzie Ridley
Samuel Bell
Yong Yan

September 2022

Prepared by
OAK RIDGE NATIONAL LABORATORY
Oak Ridge, TN 37831
managed by
UT-BATTELLE LLC
for the
US DEPARTMENT OF ENERGY
under contract DE-AC05-00OR22725

CONTENTS

ABSTRACT

The process to develop and qualify nuclear fuels for commercial nuclear application requires fundamental material development, characterization, and design; out-of-pile testing on unirradiated materials; integral fuel rod irradiations, testing, and post irradiation examinations (PIEs); and transient analyses. The historical approach depends on the generation of large empirical datasets and series of integral fuel rod irradiations, and this approach ultimately takes approximately 20 years—or sometimes longer—to acquire data through extensive sequential testing. Thus, the qualification and eventual deployment of new fuel systems constitute a long and drawn-out process. However, recent technological advancements have provided researchers the opportunity to perform out-of-cell, in-situ measurements to assess material performance for the duration of the experiment. One such example of this capability is the use of digital image coordination and thermal imaging to assess Zircaloy cladding performance under a simulated loss-of-coolant accident (LOCA) transient condition. In general, the in-situ measurements provide high-fidelity strain, strain rates, and temperature surface maps. This is critical for the United States nuclear industry, which is actively developing a technical basis to support extending the peak rod average burnup from 62 to ~75 GWd/tU and the deployment of accident-tolerant fuel. However, the Nuclear Regulatory Commission, through their research information letter, outlined a number of technical issues for the industry to address before extending burnup. One topic of specific interest is understanding the cladding balloon and rupture geometry during the LOCA heatup phase. Leveraging these advanced in-situ capabilities, this work intends to use in-situ data generated from a simulated LOCA in the Severe Accident Test Station at Oak Ridge National Laboratory to better understand high-temperature creep and its impact on Zircaloy balloon and rupture performance. This work used the BISON fuel performance code to compare BISON's high-temperature creep model predictions to in-situ data and identify limitations and gaps within the model. Additionally, BISON will subsequently be used to simulate relevant high-burnup LOCA tests. The results will be analyzed and compared to the available post-test data in a manner consistent with the approach outlined in the Nuclear Regulatory Commission research information letter.

1. INTRODUCTION

Loss-of-coolant accidents (LOCAs) are among the most severe design basis events that a nuclear power plant could experience: they are truly core-wide events affecting all fuel rods. A LOCA occurs when the primary coolant system suffers a catastrophic failure, resulting in the loss of reactor coolant. LOCAs are broken down into three subcategories: small, medium, and large break LOCAs. The most severe (and least probable) accident-initiating event is a double-ended guillotine break between the reactor vessel and main circulation pump. An example of a pressurized water reactor (PWR) fuel rod response during a double-ended guillotine break is illustrated in Figure 1 [1]. Following rupture of the cold leg, reactor coolant flashes to steam and blows down through the ruptured opening. Fission product decay heat continues to heat the fuel and reactor internals in the wake of coolant loss, further motivating the need to establish long-term cooling to mitigate the accident. Reactor depressurization occurs from LOCA initiation and completed discharge ~20–30 seconds into the transient. Once depressurized, the emergency core cooling system (ECCS) initiates to successfully pump water into the reactor primary vessel (RPV). Initially, the ECCS is unable to provide sufficient cooling to the fuel elements, and during this time interval, decay heat continues to increase fuel rod temperatures [1] such that permanent fuel damage may occur (i.e., ballooning, burst, and ultimately oxidation and hydriding), resulting in the loss of post-quench ductility (PQD) [2]. The severity of the LOCA transient is governed by a number of conditions related to the local fuel rod and assembly conditions. For example, the pre-transient rod power governs fuel rod decay heat, radial heat transfer across the pellet, gap, and cladding, external fuel rods acting as additional heat sources, and pre-transient and transient thermal hydraulic conditions. The ECCS response also is critical to governing LOCA performance.

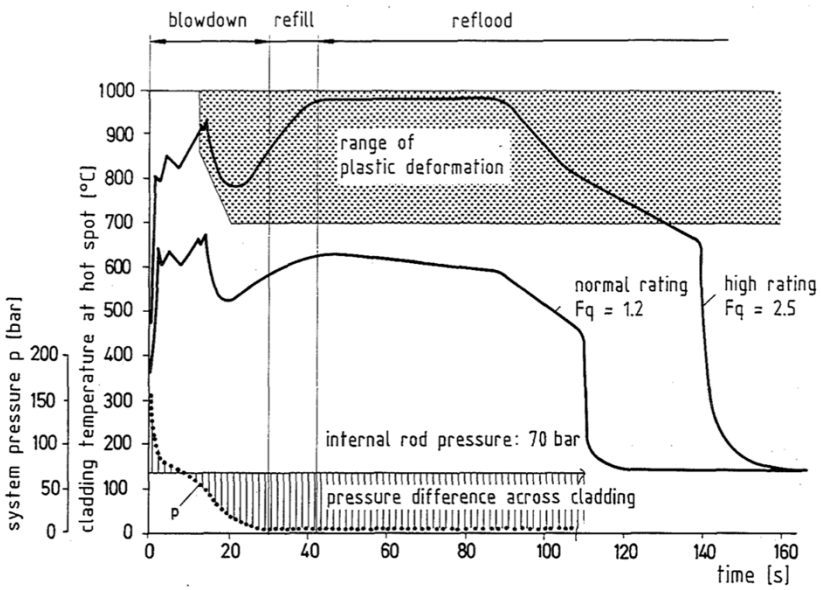

Figure 1. Generic description of Zircaloy-4 fuel rod response during a double-ended cold leg break LOCA [1].

Historically, LOCA safety analyses have been specifically tailored to prevent catastrophic fuel rod failure and ensure that the core remains controllable and amenable to long-term cooling. This approach relies on the ability of Zircaloy to maintain ductility following the reflood, or quench, phase. PQD of Zircaloy has been determined experimentally by exposing cladding ring samples to steam (<1,204°C) for a period of time before quenching the sample at some temperature <800°C. Cladding ductility is measured by performing a ring compression test and measuring the accumulation of permanent strain before failure at ~135°C and a predefined displacement rate of 0.033 mm/s [1]. In short, these data suggest that PQD can be maintained, provided the oxide thickness or hydrogen concentration remains below an acceptable value and the peak cladding temperature (PCT) remains below 1204°C. These requirements are outlined in 10 CFR 50.46. Note that cladding burst behavior is not licensing criteria. These requirements have been sufficient to adequately protect public safety for existing operating practices; however, the US nuclear industry plans to extend the peak rod-average burnup beyond 62 GWd/tU. Extending burnup introduces new technical challenges where existing guidance may no longer be applicable. The most prominent technical challenge is associated with fuel fragmentation, relocation, and dispersal (FFRD), as well as its potential consequences.

FFRD was originally observed in high-burnup LOCA experiments performed at the Halden Boiling Water test reactor. These test where originally designed to evaluate the impact of relocated fuel on local cladding temperatures; however, a LOCA test performed on fuel with a rodlet average burnup of ~92 GWd/tU experienced extensive fragmentation to the point of pulverization, termed *high burnup fuel fragmentation* (HBFF). Ultimately, the pulverized material relocated into the balloon region and dispersed through the cladding rupture opening. Since then, high-burnup LOCA test programs have investigated this phenomenon and determined a burnup range (62-75 GWd/tU rod average) in which HBFF becomes relevant [9]. These experimental observations coupled with the US nuclear industry's desire to extend burnup prompted the US NRC to release a research information letter to provide a basis to limit FFRD throughout the core based on interpretations of experimental findings.

The NRC Research Information Letter (RIL) summarizes the Office of Nuclear Regulatory Research's interpretation of FFRD experimental findings with the goal to define conservative thresholds for FFRD phenomena. The RIL highlights five elements with supporting technical basis for industry to consider in

their FFRD safety analysis. The elements are as follows: (1) fragmentation and pulverization threshold, (2) local cladding strain threshold, (3) mass susceptible to dispersal, (4) impact of transient fission gas release on balloon burst behavior, and (5) basis to support packing fractions in the non-dispersed balloon region. The industry is pursuing multiple approaches to address FFRD from a safety analysis perspective. The simplest approach is to prevent burst from occurring; however, if burst does occur, then cladding performance (rupture timing, balloon size, and rupture size) will have a significant impact on FFRD and its consequences. Therefore, it may be critical to accurately model cladding ballooning during a LOCA. Modeling efforts to date have prioritized accurately predicting burst timing using the chapman failure correlation. Comparisons between the calculated and experimentally measured balloon strains have been made, and in general, the modeling results grossly under-predict post burst peak cladding balloon strain (i.e., hoop strain). General consensus suggests uncertainty in code predictions are related to varying experimental surface conditions, such as azimuthal or axial temperature gradients, that cannot be accurately captured due to a lack of experimental data.

Recent work at Oak Ridge National Laboratory (ORNL) used digital image correlation and infrared thermography to assess Zircaloy cladding performance under a simulated loss-of-coolant transient condition. In general, the developed capability provides high-fidelity time- and spatially dependent strain, strain rates, and temperature measurements. Therefore, this work intends to leverage in-situ data generated from a simulated LOCA in the Severe Accident Test Station at ORNL to validate the BISON fuel performance code and the Zircaloy high-temperature creep model predictions. Additionally, model limitations are identified and discussed. Lastly, BISON is validated for a simulated high-burnup LOCA test performed at ORNL.

2. VALIDATION TO IN-SITU CLADDING BURST TESTS

2.1 DIC BURST TESTS SUMMARY

Eight digital image correlation (DIC) tests were performed at ORNL under the AFC program, and five additional tests were identified from the literature [3–5]. The nominal pre-transient geometry for each test was 9.5 mm outer diameter, 0.575 mm wall thickness, and 76 mm length (the shortened length will be discussed below). The test from literature had a length of ~210 mm. For the ORNL test, cladding deformation was monitored through a ~38 mm hole bored through the side of the infrared (IR) furnace. This afforded direct line-of-sight of the cladding tube through the viewing chamber. However, the cladding segment was shortened from the standard ~300 mm to 76 mm to ensure that the balloon evolution was visible. A thick-walled 316SS extension tubing was used to center the cladding directly in front of the viewing chamber. Each test was performed in air due to the quartz reaction tube emitting IR as the temperature increased, rendering the cladding no longer visible. Finally, a SiC shell was used to smooth out the axial and azimuthal temperature profiles by preventing direct reflection of the IR lamps off the cladding surface. This addition allowed for accurate quantification of the cladding temperature along the axis as the IR reflections were no longer present. Table 1 and Table 2 summarize the ORNL and literature DIC tests. A key difference between the test described in Table 1 and Table 2 is that Table 2 used an internal tungsten heater as opposed to an external IR furnace.

Table 1. Burst DIC Test Matrix.

Material	Specimen Length (mm)	Heating Rate (°C/s)	Heating Type	Initial Pressure at 20 °C (MPa)	Pressure Valve
Zry-4	76	1	External IR	6.2	Closed
				8.2	Closed
				10.3	Closed
				15.6	Closed
				6.2	Open
				8.2	Open
				10.3	Open
				15.6	Open

Table 2 DIC Tests from Literature

Material	Specimen Length (mm)	Heating Rate (°C/s)	Heating Type	Initial Pressure at 20 °C (MPa)	Pressure Valve	Reference
Zry-4	210	~1	Internal Tungsten Heater	7	Open	3
		1		8	Open	4
		14		8	Open	4
		28		8	Open	4
		~1		7	Open	5

2.2 MODELING APPRAOCH

DIC LOCA tests outlined in Table 1 and Table 2 are intended to provide highly characterized data from a highly controlled test. The highly characterized data are intended to be used in a fuel performance code to provide time-dependent validation of the fuel performance codes models. The BISON fuel performance code was used for the LOCA simulations described herein, based on previous validation of the code for LWR applications [10–12]. BISON was built upon the Multi-Physics Object-Oriented Simulation Environment (MOOSE) framework, a parallel finite element computational system [13]. MOOSE uses the Jacobian-free, Newton–Krylov (JFNK) method to solve fully coupled systems of nonlinear partial differential equations. In addition, BISON can be parallelized to perform high-fidelity modeling of fuel rods in three dimensions, as well as in full-length R-Z and planar slice geometries. BISON has been extensively validated for both LWR steady state [14] and transient [15] integral tests. The models used for these validation efforts are well documented [14,15], as are the implementations of these models in BISON [6]. Table 3 summarizes the models used in BISON analysis as well as the associated references. The model leverages BISON's R-Z capability with the following geometric properties: 9.5 mm outer diameter and 0.575 mm wall thickness. The cladding length was different for the two different test conditions, and the BISON model accounts for these differences.

Table 3. Summary of the BISON Models and Associated References relevant to FFRD

Fuel			Cladding		
Property	**Model**	**Reference**	**Property**	**Model**	**Reference**
Thermal Conductivity	NFIR	[17,18]	Thermal Conductivity	Fink	[26]
Elastic Properties	MATPRO	[19]	Elastic Properties	MATPRO	[19]
Fission Gas Release	Sifgrs	[20]	Thermal Expansion	MATPRO	[27]
Thermal Expansion	Constant	[21]	Thermal Creep	Limback-Anderson and Erbacher	[19]
Pulverization	Turnbull	[33]	Rupture Criteria	Chapman / Strain Rate	[28,29]
			Rupture Opening	NEAMS	[31]

The main consideration beyond tube geometry is associated with the simulated boundary conditions. The DIC tests were developed with this in mind. Rod internal pressure was experimentally measured during the test by a pressure transducer. In a true validation framework, the initial pressure at a specified temperature would be calculated by BISON; however, the purpose of this comparison is to completely isolate the high-temperature creep model. Therefore, the experimentally measured pressure was directly applied to the inner surface of the tube. Peak cladding temperature was measured using a thermocouple located on the top of the cladding tube. An example of the measured pressure and peak cladding temperature is shown in Figure 2. The axial temperature profile was determined by using an IR camera, where the thermocouple measurement provides a reference temperature for the IR camera. Two predominant axial temperature profiles were measured during the DIC tests; see Figure 3. Figure 3 reports these temperature profile in terms of a normalized value in accordance with the thermocouple measurement. The axial profiles shown in the figure are a direct result sample location within the furnace, the hole in the furnace contributing to a local depression in the middle of the tube, and the SiC shell to normalize azimuthal temperatures. The appropriate axial temperature profile was applied to the exterior cladding surface for each DIC simulation. Lastly, the DIC test were unique insofar as the top and bottom of the tube were fixed, requiring the application of the appropriate BISON boundary conditions to prevent unrealistic axial displacements.

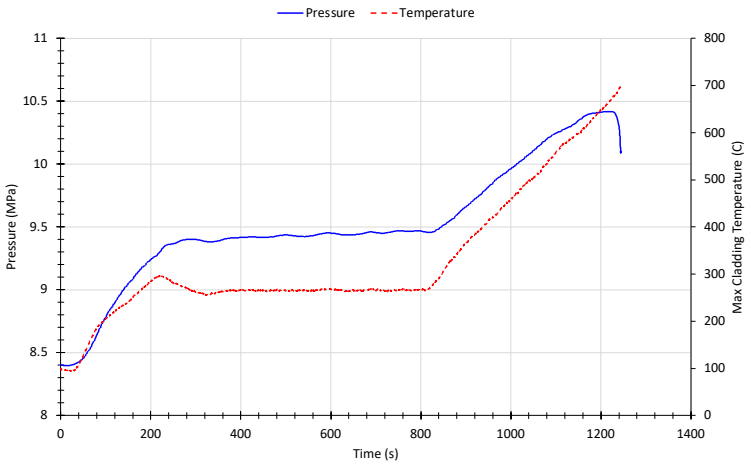

Figure 2. Time-dependent pressure and maximum temperature measurements during DIC LOCA test.

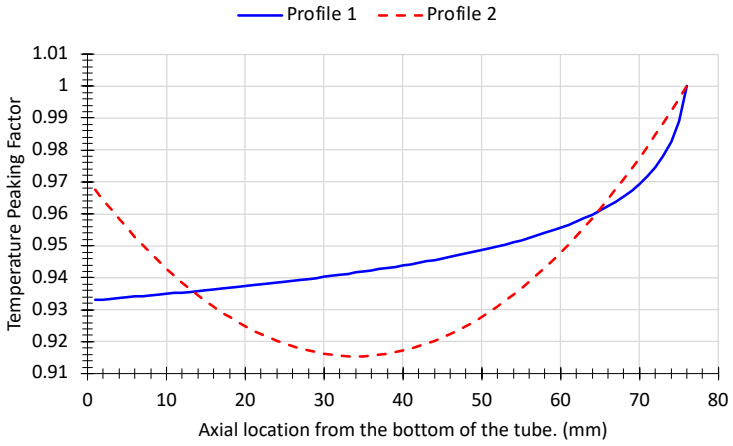

Figure 3. Cladding surface peaking factors measured by the IR camera at the time of burst.

High-Temperature Creep Model

The high-temperature cladding creep model implemented into BISON was first documented by Erbacher et al. [1] in 1980. The model was developed from isothermal uniaxial tension tests conducted in an inert atmosphere. The samples were directly heated with either a joule or ohmic system. A hydraulic system was used to apply a constant uniaxial load to the sample and measure strain under constant temperature and load conditions. Strain was determined by assessing the displacement of the hydraulic system as a function of time. The creep test was terminated after a 10 min time interval or a total strain of 0.15 (15%). There are multiple concerns with the use of these data in LOCA applications. First, Zircaloy is an anisotropic material in nature. Nuclear-grade Zircoloy tubes are inherently anisotropic as a result from the crystal structure. Secondly, cladding burst tests inherently apply a biaxial stress state to the cladding tube material under both dynamic temperature and pressure (stress) conditions. The data generated through the uniaxial tension test generate steady-state axial creep data under isothermal conditions, and, therefore, these data are applicable only under steady-state conditions in the axial direction. Furthermore, tube pressures in high-burnup fuel rods range from 8 to 15 MPa, and possibly higher in some cases. Using thin wall approximation, the stress in both the hoop and axial direction can range ~70 to 125 MPa and 25 to 60 MPa, respectively. However, the uniaxial creep data focus on low stresses (<60 MPa) at temperatures >700°C, and this trend holds true for biaxial creep data as well [7]. This strongly suggest these data will not be applicable to simulated LOCA conditions with high rod internal pressure like those expected in high-burnup fuel. Nonetheless, the uniaxial tensile data were used to generate the isotropic material parameters for uses in the following creep equation:

$$\dot{\epsilon}_{eff} = A exp\left(\frac{-Q}{RT}\right)\sigma_{eff}^{n},$$

where $\dot{\epsilon}$ is the effective creep strain rate, A is the strength coefficient in units of $MPa^{-n}\ s^{-1}$, Q is the activation energy in J/mol, T is the temperature in K, σ_{eff} is the effective stress in MPa, and n is a dimensionless stress exponent. The data discussed above was used to estimate the material parameters for use in the creep equation shown in Table 4. More details of steady-state uniaxial creep testing can be found in Rosinger et al. [8]. Information related to biaxial steady-state creep testing can be found in Donaldson and Healey [7].

Table 4. Zircaloy 4 High-Temperature Creep Material Parameters [8]

Zircaloy Phase	Creep Rate Regime	A ($MPa^{-n}\ s^{-1}$)	Q (J/mol)	n

α phase	—	8737	$3.24e5 + 24.69(T - 923.15)$	5.89
Mixed α − β phase	$\dot{\epsilon}_{eff} \leq 3e-3$	0.24	1.02366e5	2.33
Mixed α − β phase	$\dot{\epsilon}_{eff} \geq 3e-3$	Interpolation	Interpolation	Interpolation
β phase	—	7.9	1.41919e5	3.78

2.3 BISON VALIDATION OF EXPERIMENTAL DATA

The BISON fuel performance code and creep model described above were used to evaluate all DIC burst tests described in Table 1 and Table 2. However, specific cases are discussed here to highlight differences between simulations with low and high pressure and heating rates. A mechanistice creep model should take into consideration of the the cladding stress state, temperature, or heating rate; therefore, evaluating bounding conditions should provide a reasonable summary of the model's capabilities.

Figure 4 compares BISON modeling predictions to the experimentally measured DIC data for a 6.2 MPa open valve test. This case was selected for comparison because the pressure was held constant for the duration of the test. This ensures that the comparison is performed such that the creep model predictions are fully isolated at a specific rod internal pressure. The first observation is BISON generally over-predicts the experimentally measured values. The experimental values at temperatures lower than ~600°C likely have larger uncertainties due to the laser engravings (pattern fidelity) on the Zry-4 as well as potential heat waves causing changes in the optical path. In the future, a speckled pattern from high-temperature spray paint will be used increase fidelity of the DIC tracking field and reduce experimental uncertainties. However, BISON clearly over-predicts strain deformation above ~600°C to the point where the terminal strain values are ~25% greater than the experimentally measured value. Another interesting observation is related to the axial strain results. Generally, the measured axial strain vales are near zero. This is related to the restraint applied to the top and bottom of the test train. The restraint is not perfect, and, therefore, slight increases in the axial strain are observed. Perfect restraint of the test train would look similar to the BISON results with the axial strain being effectively zero until ballooning occurs. The axial strain becomes negative as large balloon deformation occurs. As the balloon radially expands, the tube is expected to axially contract—a behavior captured by BISON. In general, some work may be required to improve the model as it relates to low-pressure conditions. However, it could be argued that the difference between the code predictions and experimentally measured values fall within an appropriate deviation, and additional data may result in slight under-predictions.

Figure 5 presents similar results to those shown in Figure 4; however, the results in Figure 5 reflect a constant high pressure (15.1 MPa) SATS test. 15.1 MPa is intended to represent a near upper bound rod internal pressure that could be experienced by high-burnup (>62 GWd/tU rod average) fuel. Unlike the lower pressure comparison in Figure 4, BISON shows more deviation from the experimentally measured values, specifically hoop strain. This is not surprising, as the creep model was developed from uniaxial creep test where the applied stress is much lower than that imposed on the cladding. Therefore, when extrapolating the empirical model to higher stresses, it would make sense for the model to either over- or under-predict the experimental results. This deviation indicates that the current model is not appropriate for handling extreme pressure regimes, and model development is needed to more accurately capture high-pressure burst conditions. The deviation in the axial data in Figure 5b is a result of the high pressures and transient conditions impacting the test strain stability. Again, a perfect constraint would lead to a near zero axial strain until ballooning occurs.

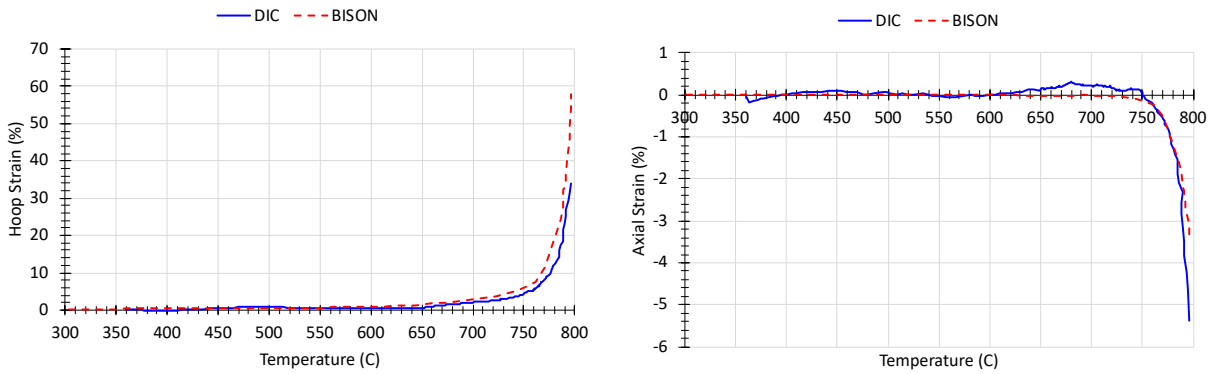

(a) (b)

Figure 4. BISON a) hoop strain and b) axial strain comparison DIC measurements from a constant low pressure (6.2 MPa) DIC test.

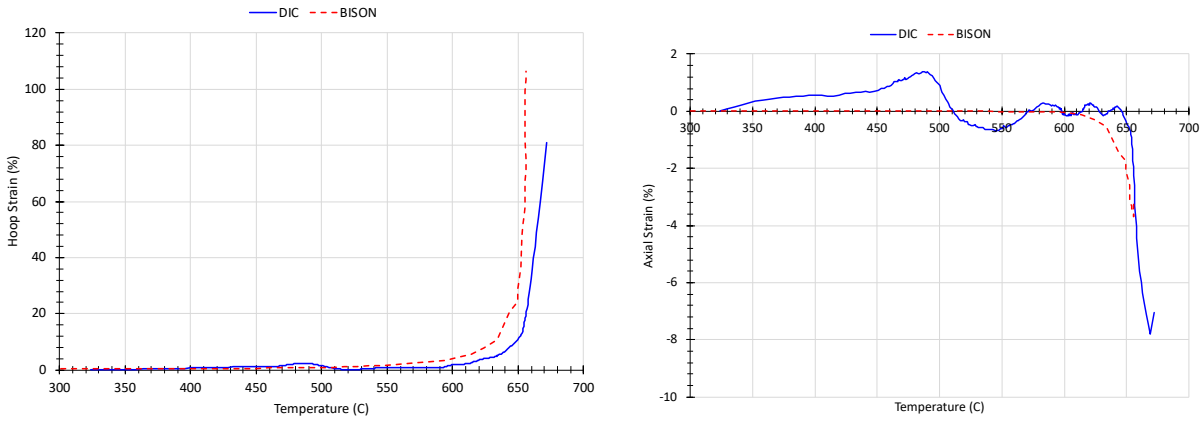

(a) (b)

Figure 5. BISON a) hoop strain and b) axial strain comparison DIC measurements from a constant high pressure (15.1 MPa) DIC test.

A second comparison is shown in Figure 6. Here, the pressure is held constant at 8 MPa, and the heating rate is varied. The heating rate in Figure 6a is 1°C/s whereas the heating rate in Figure 6b is 28°C/s. The results in Figure 6a show good agreement between BISON predictions and the experimental data, however, the results do disagree as temperature increases likely due to tertiary creep. This again is not surprising, as the data used to develop the creep model are from a slow experiment lasting ~15 min with similar stress conditions. However, the model performs poorly in the higher heating rate conditions; see Figure 6b. The model initially over-predicts strain. This behavior continues until the experimental data suggest the presence of plastic instability, resulting in rapid changes in the strain behavior. BISON predictions suggest a slower strain response than the experimental data, and, furthermore, the trend of over-predicting reverses as temperature increases. This points to a heating rate model deficiency and impacts the ability of the empirical model to accurately predict balloon deformation under high heating rate conditions.

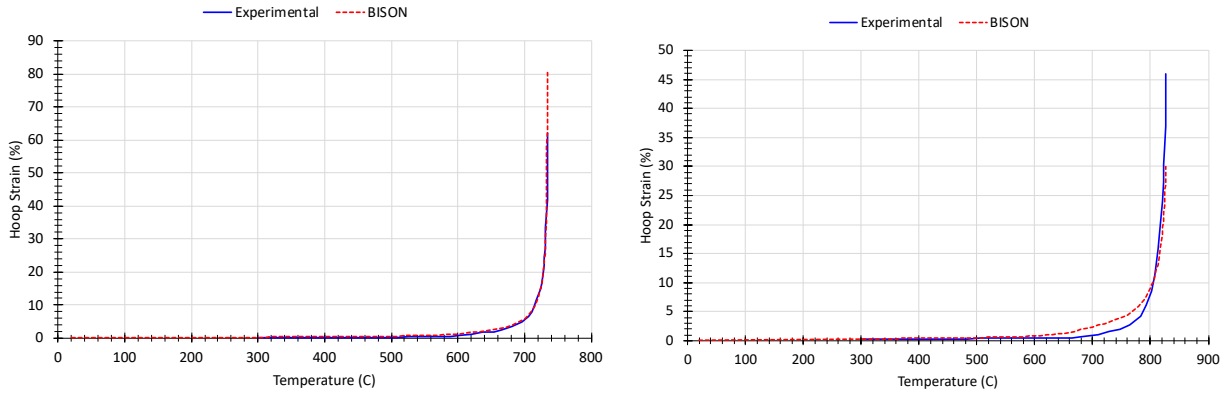

Figure 6. BISON hoop strain comparison as a function of heating rates to DIC measurements from a constant pressure (8 MPa) DIC tests a) 1°C/s and b) 28°C/s.

The results discussed above compare two similar cases to each other; however, in reality, cladding balloon and burst behavior are statistical in nature. Therefore, BISON was used to assess every case reported in Table 1 and Table 2 to determine the difference between the BISON results and the experimental data from a broader statistical evaluation. BISON results and experimental data were extracted at the same at temperatures for direct one-to-one comparison. The percent difference was determined by subtracting the experimental data from the BISON predictions and dividing by the measured data. This comparison illuminates differences between the model predictions and identify modeling gaps or areas of high uncertainties within the model. Figure 7 illustrates this comparison as a function of temperature. Additionally, the data are broken down into various components as identified by the discussion above, where blue circles represent heating rates greater than 1°C/s, red triangles represent pressures greater than 9 MPa, and green squares represent data where the heating rate equals 1°C/s and the internal pressure is less than 9 MPa. In general, there is significant scatter in the data: most of the data suggest BISON over-predicts the experimentally measured data. Again, the experimental data at temperatures <500°C may be subject to measurement uncertainties given that the measured strain values are close to 0.1%. However, trends in the data become clear. BISON over-predicts (>100%) high heating rates (> 1°C/s) at lower temperatures; however, the trend reverses as the temperature increases, as shown in Figure 6b. The most notable trend is observed for high rod internal pressures (>9 MPa). BISON does a reasonable job of predicting strains at lower temperature. However, as the temperature exceeds ~500°C, BISON over-predicts the experimental results by 200%. This is not surprising because BISON generally over-predicts strain; moreover, the model's range of applicability does not extend to high pressures (>9 MPa). The model is in effect extrapolating from its range of applicability to the high-pressure conditions, and as the results show, the extrapolation further deviates from the experimental data. However, the model does a reasonable job of predicting strain evolution where the heating rate equals 1°C/s and the pressure is less than 9 MPa. The culmination of these results suggests the high-temperature creep model currently used in BISON needs improvement. The first-order improvements are to ensure that the model better handles higher heating rates (i.e., >1°C/s) and higher pressures (>9MPa). The second-order improvements are for the model to consider microstructure evolution before and during the LOCA transient.

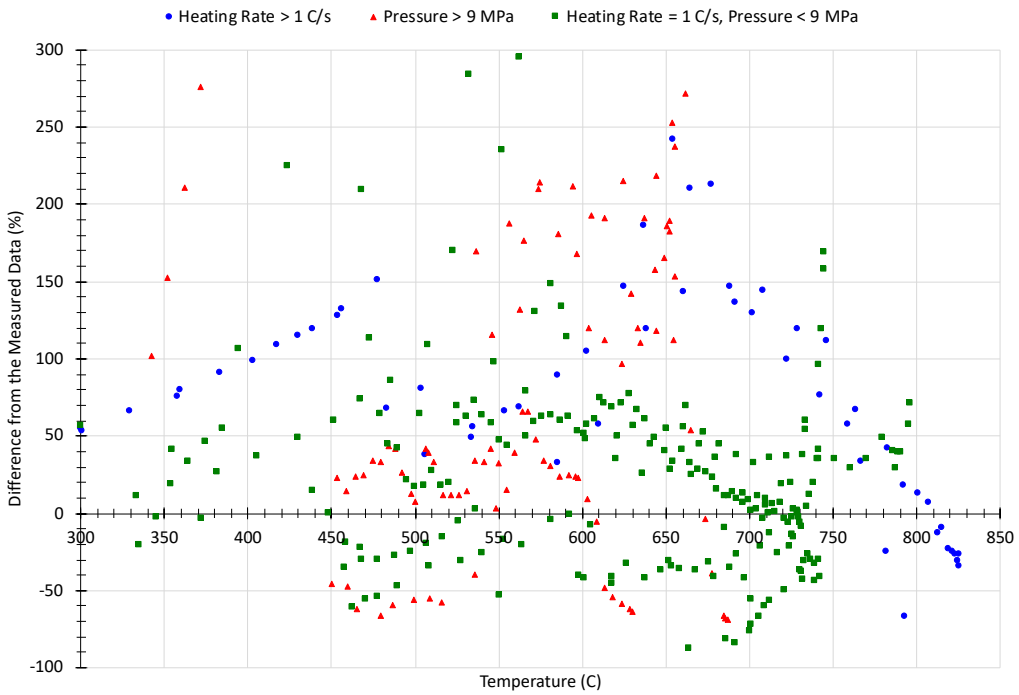

Figure 7. Percent difference between the BISON predictions and experimentally measured (P-M)/M.

Lastly, BISON stress and strain rate-based failure and hoop strain predictions were compared to the experimentally measure values in Table 5. The stress-based failure model is model reported in NUREG 0630 [1], whereas the strain rate failure model occurs when the strain rate is greater than 2.78 %/s [34]. The stress-based failure model generally predicts a lower failure temperature than the strain rate failure model for a heating rate of 1 ^{o}C/s and certainly under predicts hoop strain. The strain rate model does a failure good job of predicting failure, and hoop strain results are poor with the exception of two cases. There are a number of cases where the strain rate failure model does not predict failure. This, however, should not reflect on limitations of the failure model, but highlights the limitations within the creep model. The takeaway of these results indicates the strain rate failure models provides better predictions with respect to the experimental data. However, the behavior reverses as heating rate increases. This is to be expected as the strass-based failure criteria is a function of heating rate, while the strain rate failure criteria does not have a heating rate dependence. This suggests additional data is needed in order to refine the applicability of the strain rate failure model.

Table 5. BISON rupture predictions in comparison to the experimentally measure values

Initial Pressure at 20 °C (MPa)	Pressure Valve	Heating Rate	Experimental Rupture Temperature (°C)	Experimental Rupture Strain (%)	Rupture Temperature (°C) – Stress Based Failure	Rupture Strain (%) - – Stress Based Failure	Rupture Temperature (°C) – Strain Rate Based Failure	Rupture Strain (%) - – Strain Rate Based Failure
6.2	Open	1	796	34	771	11	791	34.8
7	Open	1	687*	68	N/A	12	N/A	12
7	Open	1	642*	100	N/A	12	N/A	12
8	Open	1	735	62	703	6	711	8.3
8.2	Open	1	751	84	720	10.3	741	46.6
10.3	Open	1	687	49	674	7.8	N/A	15.1
15.9	Open	1	671	66	566	2.2	652	47.5
6.2	Closed	1	739	34.5	N/A	12	N/A	12
8.2	Closed	1	703	58	662	6	N/A	16.4
10.3	Closed	1	681	62	674	7.8	N/A	15.1
15.9	Closed	1	631	30	545	1	N/A	10.9
8	Open	14	793	40	776	16	768	5
8	Open	28	826	46	802	23	781	6

***Sample was not heated to rupture due to internal tungsten heater**

3. BISON VALIDATION TO HIGH BURNUP LOCA TEST

3.1 HIGH BURNUP LOCA TESTING AT ORNL

The Severe Accident Test Station (SATS), which is installed at the Irradiated Fuels Examination Facility (IFEL)—a hot cell facility in at ORNL—is an integral test facility capable of studying the response of irradiated fuels and materials under design basis accident (DBA) and beyond design basis accident (BDBA) scenarios. The motivation behind the development of this capability is restoring the US capability to perform semi-integral LOCA testing on irradiated materials. An overview of the test station prior to in-cell insertion can be found in Capps et al. [9], and Table 6 summarizes the range of test parameters for each type of SATS test.

Table 6. Summary of test parameters for each module and test type

	DBA module		**BDBA module**
	LOCA integral test	**Oxidation-quench test**	**High-temperature test station**
Sample spec	Fueled rod	Defueled rod	Rod or coupon with 3 mm hole
Sample segment, mm	~200–300	~25–50	~25–50
Pressure, MPa	~8, max 20	0.1	0.1
Max temp, °C	1200	1200	1700
Heating rate, °C/s	5	5; max 20	.25; max .33
Steam flow rate, $mg/cm^2 \cdot s$	~5.7	~5.7	3.0–7.0
Gas environment	Steam or argon	Steam or argon	Steam or argon
Quench, °C	@ 20–800	@ 20–800	None
Quench condition	Rising water around sample	Rising water around sample	None
Quench flow rate, mm/s	≥15	≥15	None
Test time, min	≥30	≥30	Multiple days

This strategic capability emerges as the US nuclear power industry is under financial duress due to low natural gas prices; as a result, several plants have shut down. The nuclear industry has since progress toward extending burnup beyond 62 GWd/tU in an effort to reduce operational cost and alleviate financial duress. However, the US NRC has identified FFRD as a key issue to be addressed for burnup extension. To date, three high burnup LOCA tests have been performed in SATS [9].

The high burnup test specimens were assembled with two Type-S thermocouples strapped to the outer surface of the cladding at approximately ~5 cm above the sample centerline. The LOCA tests were conducted in a steam environment at 1,000°C, but without water quench. The full LOCA sequence is as follows:

- heating in flowing steam to 300°C and pressurizing fuel segment to 1,200 psi
- heating in flowing steam at 5°C/s from 300°C to 1,000°C
- holding in steam for 120s at 1,000°C
- cooling at 3°C/s to 800°C
- furnace cooling from 800°C to room temperature

Figure 8 highlights the experimentally measured temperature and pressure from the North Anna 1 high burnup LOCA test.

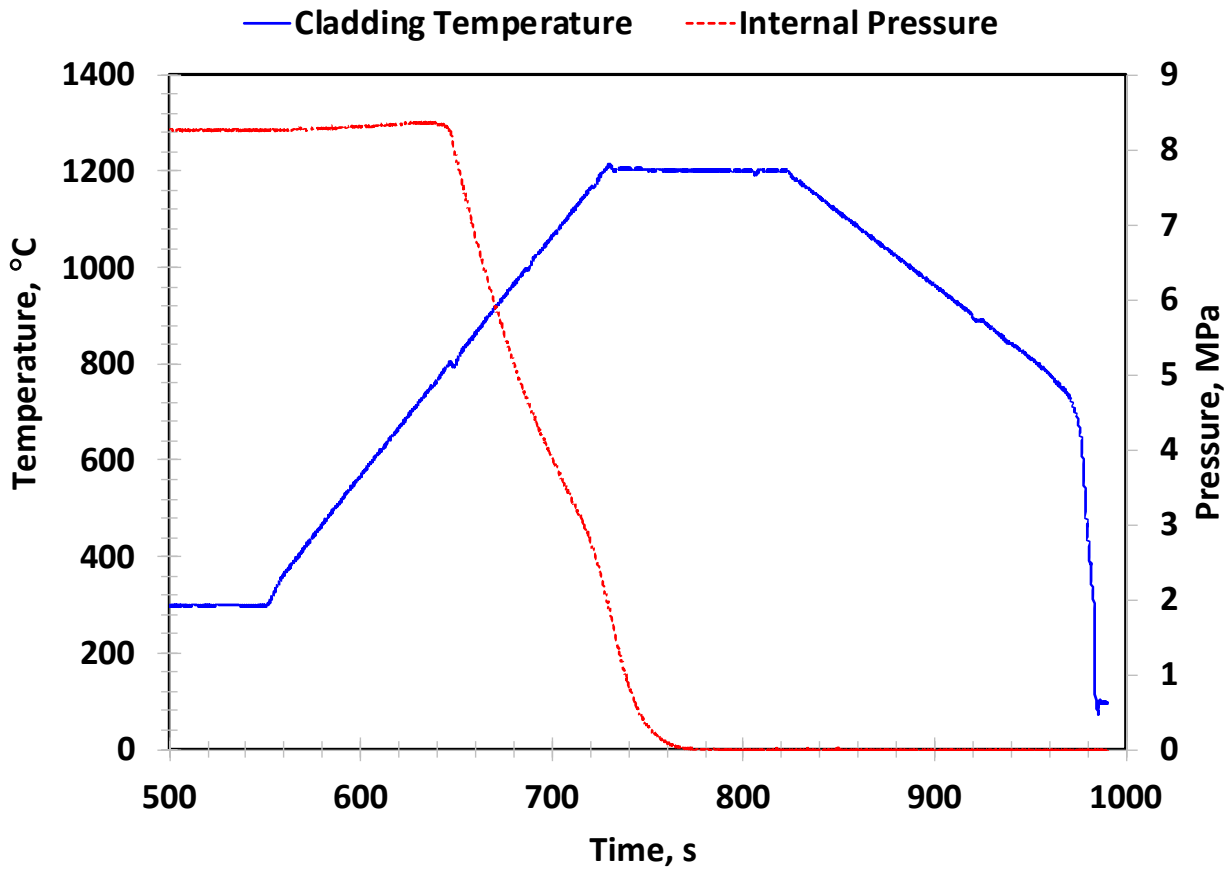

Figure 8. Cladding temperature and tube pressure recorded during the North Anna 1 high burnup LOCA test [9]

3.2 BISON VALIDATION OF EXPERIMENTAL DATA

3.2.1 HB Robinson

A high burnup fuel rod segment was harvested from a fuel rod irradiated in the HB Robison PWR for post-irradiation examination (PIE) and subsequent LOCA testing. The characteristic fuel rod geometry is shown in Table 7. The fuel rod design is specific to a 15×15 fuel assembly design, and it should be noted that this fuel rod is of an older design. More modern PWR fuel designs consist of thinner cladding tubes, smaller outer diameters, and modern cladding alloys. The fuel rod properties shown in Table 7 were used to develop a representative BISON model to provide accurate fuel performance and depletion results prior to simulating the LOCA test results. The rodlet was harvested from the axial location spanning 2.54 to 2.84 m from the bottom of the fuel rod. This segment was specifically chosen due to the relatively flat burnup profile as well as the local power being slightly higher than the rod average linear heat rate. The fuel rod power history was extracted from Gerczak et al. [32] and reproduced in Figure 9. The fuel rod was operated irradiated for five cycles in a relatively low power location. After the five cycles, the rod was pulled out and inserted into a new assembly for a sixth and seventh cycle until its final discharge in 1995.

The rodlet operational history is such that one would expect the fuel temperatures and fission gas release to be low. BISON fuel centerline and periphery temperatures predictions confirms this hypothesis; see

Figure 9. The fuel centerline temperature follows the linear heat rate (LHR) as one would expect, whereas the pellet periphery temperatures decrease to a near-equilibrium temperature ~75°C higher than the reactor coolant temperature. The pellet periphery temperature evolution is constant with gap closure occurring early in life. BISON predicts minimal FGR, whereas the experimentally measured FG on a full-length fuel rod was 2.1% [32]. Subsequently, BISON was used to simulate the SATS LOCA test of this rodlet to assess fuel fragmentation predictions. Details about the HB Robinson test conditions can be found in Capps et al. [9].

Two different rupture models were considered for the BISON evaluation. The first leverages a stress-based failure criteria developed and used by the NRC [28], whereas the second model uses the cladding strain rate to determine failure [29]. The two models should result in different cladding deformation at rupture and provide a lower and upper bound on predicted cladding deformation. Cladding rupture during the experiment occurred at 770°C, and both failure models over-predicted the rupture temperature: 780°C and 787°C with the stress-based failure criteria being lower. However, the predicted peak cladding deformation behavior for both rupture conditions is significantly differs from the experimentally measured value; see Figure 10. BISON predictions suggest the peak cladding hoop strain will remain below 10%, whereas the experimental data doubles the BISON predictions. This suggests BISON is not accurately accounting tertiary creep as well as tertiary creep's impact on cladding deformation. This, however, would only be useful if the strain-rate failure criteria were being considered as the stress based approach fails before tertiary creep could occure. It should be noted that transient fission gas release (tFGR) is not considered in the LOCA simulation. However, the measured rod internal pressure was directly applied to tubes inner surface; therefore, any tFGR would have been captured in the simulation.

Table 7. HB Robinson segment characteristics used to develop BISON steady state and transient models

Reactor Type	PWR
Initial Enrichment (wt. % U-235)	2.9
Segment Avg. Burnup (GWd/tU)	71
Discharge Year	1995
Cladding Type	Zircaloy 4
Cladding Outer Diameter (mm)	10.76
Wall Thickness (mm)	0.76
Pellet Outer Diameter (mm)	9.06
Pellet-Cladding Gap Thickness (mm)	0.095

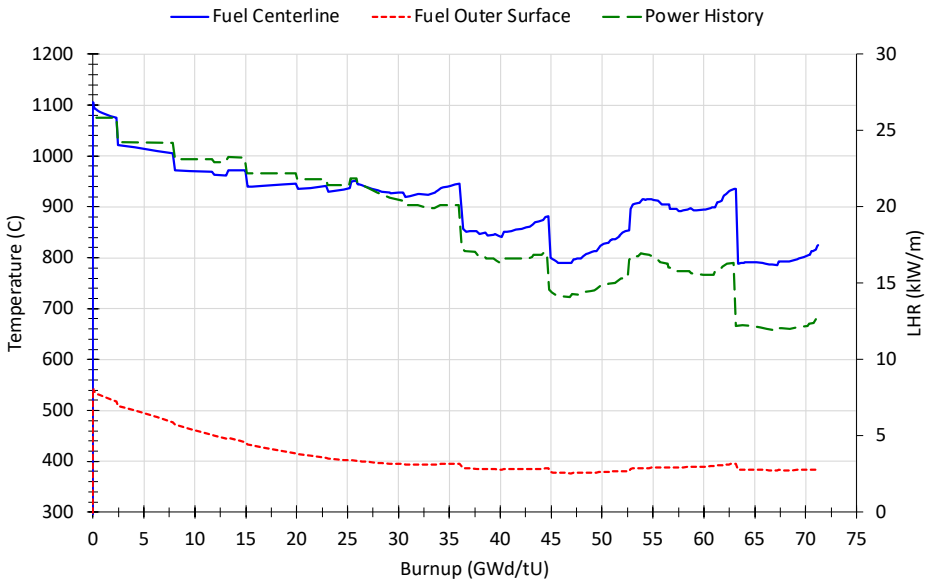

Figure 9. BISON power history and fuel temperature results as a function of rodlet average burnup [32].

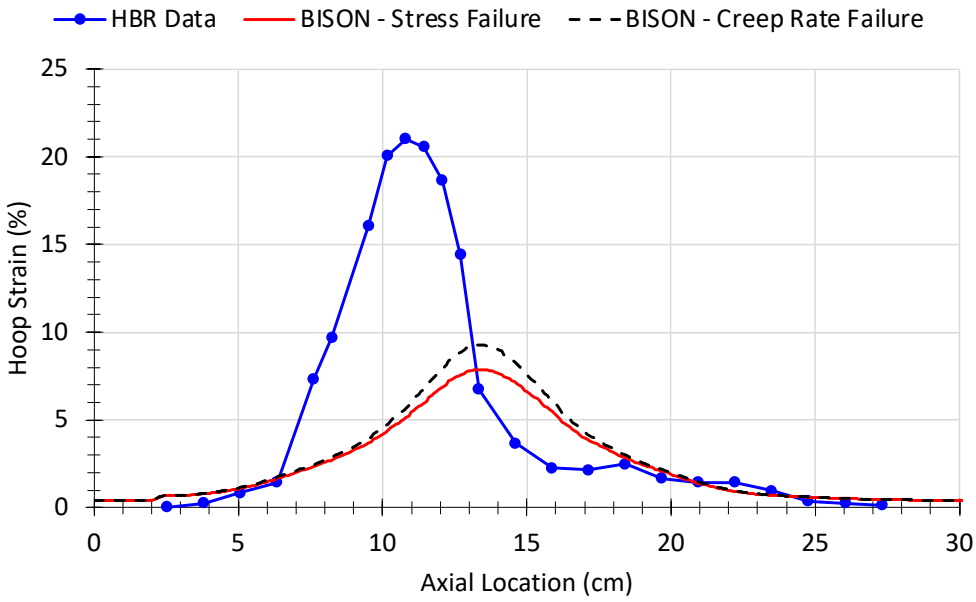

Figure 10. BISON post LOCA cladding hoop strain results for the stress based and strain cladding failure criteria [9].

The NRC's RIL outlines thresholds for calculating fuel fragmentation, relocation, and dispersal. The key thresholds of interest are for fuel fragmentation and cladding strain threshold below which fuel relocation is limited. The fuel fragmentation criteria outlined in the NRC RIL is twofold. The first, Eq. (1), is for fragments smaller than 1 mm; the second, Eq. (2), is for fragments smaller than 2 mm. The only input parameter is the local or rodlet average burnup, shown as Bu.

Mass Fraction = 0.04(Bu-55) (1)
Mass Fraction = 0.05(Bu-55) (2)

Additionally, there is a second empirical model developed by Turnbull [33] based on the local/nodal burnup of the sample as well as terminal temperature. Turnbull's model is applicable only to fragments smaller than 1mm, and for the purposes of this analysis, only fragments smaller than 1 mm are discussed. The second threshold is the cladding relocation threshold based on cladding strain. The RIL suggests fuel relocation will be mitigated provided the cladding strain remains below 3%. Table 8 shows the results of the analysis when comparing the Turnbull and RIL fragmentation criteria as well as an estimation of how much fuel will be susceptible to relocation and potential dispersal. It is clear that the RIL overestimates the amount of fragmented material, whereas the Turnbull model is within 3% of the experimentally measured data. When applying the 3% strain restriction on relocation, both results drop by a third. Note that the experimental data have a large peak value, but the hoop strain along the axis is 9 cm, whereas the BISON results are 10 cm. Therefore, this value is considered more conservative than the experimental measured value, and this holds true when comparing the experimentally measured values to the values predicted.

Table 8. Summary of the BISON Models and Associated References relevant to FFRD.

	Turnbull Fragmentation Criteria	**RIL Fragmentation Criteria (1 mm/2 mm)**
Fuel Susceptive to Pulverization (%)	30.6	64/80
Fuel Susceptible to Relocation (%)	10.2	21/27
Measured Fragmentation = 31.56% Calculated Fuel Susceptible to Relocation = 9.4%		

3.2.2 North Anna

A high-burnup fuel rod segment was harvested from a fuel rod irradiated in the North Anna (NA) PWR for PIE and subsequent LOCA testing. The characteristic fuel rod geometry is shown in Table 9. The fuel rod comes from a more modern fuel rod and assembly design, but very little is known about the operating conditions. It is estimated that the last cycle power was above 15 kW/m, and the rodlet in question was harvested from 1.83 m to 2.28 m from the bottom of the fuel rod. It would be reasonable to suggest this rodlet was operating between 19 and 21 kW/m at end of life; however, this is merely speculation. Therefore, BISON was used to evaluate only the LOCA transient portion of the evaluation.

BISON NA predictions are similar to the HB Robinson results in that BISON significantly under-predicts the peak hoop strain. Again, two failure criteria were considered in the analysis, and both under-predicted. However, there is one significant difference between the NA and HB Robison results: the NA sample ruptured at 791°C, and BISON predicted rupture to occur at 753°C (stress-based criteria) or 760°C (strain rate). The decrease in the burst prediction is related to the change in cladding thickness: HB Robinson had a 0.74 micrometer thickness, and NA has a 0.57 micrometer thickness. There may have been other factors contributing to the difference in rupture, such as oxide thickness. HB Robinson being Zirclaoy-4 had a large oxide (~100 micrometers), whereas the NA rodlet had an oxide layer of ~30 micrometers. Nonetheless, BISON still significantly under-predicted the balloon geometry, and unlike the HB Robinson results, the axial balloon geometry is less than the experimentally measured vales. This is most likely due to differences in axial temperature gradients along the tube along with a lack of tertiary creep being appropriately captured.

Table 9. North Anna segment characteristics used to develop BISON transient models

Reactor Type	PWR
Initial Enrichment (wt. % U-235)	4.2
Segment Avg. Burnup (GWd/tU)	69
Discharge Year	2004
Cladding Type	M5
Cladding Outer Diameter (mm)	9.5
Wall Thickness (mm)	0.57
Pellet Outer Diameter (mm)	8.2
Pellet-Cladding Gap Thickness (mm)	0.080

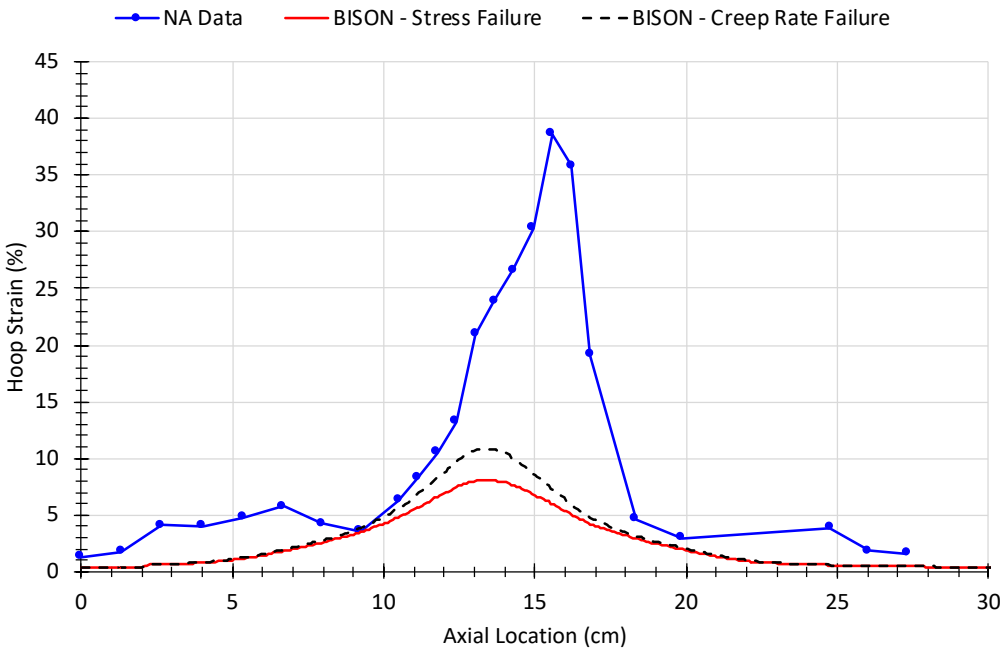

Figure 11. BISON post LOCA cladding hoop strain results for the stress based and strain cladding failure criteria.

A similar fuel fragmentation calculation was performed on the NA sample. The Turnbull model predicts similar mass fraction of fragmentation <1 mm that are within 13% of the experimental values, whereas the RIL model grossly overpredicts the amount of fragmented fuel. However, the calculated balloon geometry significantly impacts the result: the experiment balloon length was twice that calculated by BISON. Again, this may be a thermal boundary issue, and it may also be a function of BISON's inability to consider tertiary creep and predict the peak hoop strain.

Table 10. Summary of the BISON Models and Associated References relevant to FFRD

	Turnbull Fragmentation Criteria	**RIL Fragmentation Criteria (1 mm/2 mm)**
Fuel Susceptible to Pulverization (%)	23.4	56/70
Fuel Susceptible to Relocation (%)	7.8	18.7/23.3
Measured Fragmentation = 27.4% Calculated Fuel Susceptible to Relocation = 16.4%		

4. SUMMARY AND FUTURE WORK

BISON simulations were used to evaluate in-situ DIC burst tests to assess the high-temperature creep model. The results suggest the creep model does a reasonable job under very specific condition; when those conditions deviate, the model results deviate as well. Conditions for which the model showed reasonable predictions occurred when the rod internal pressure remained below 9 MPa and the heating rate was equal to 1°C/s. The model did not perform well when high rod internal pressure or heating rates were considered. Subsequently, BISON was used to simulate LOCA testing on high burnup. Cladding deformation was evaluated, and fuel fragmentation was estimated based on guidance provided by the NRC RIL on FFRD. The NRC guidance demonstrated a constant over-prediction, whereas the Turnbull pulverization model predictions were comparable to the experimentally measure data.

In general, it was determined that the existing high-temperature creep model was unable to accurately predict balloon deformation during a simulated LOCA test. It should be noted that cladding deformation has a statistical dependence, but through numerous comparisons, the model consistently highlighted major gaps within the model. The first is the models inability to accurately capture cladding behavior above 9 MPa. Again, the model was not intended for use at such high pressure; therefore, model improvements are required to broaden the application of this model to higher pressures. Secondly, the model was unable to capture cladding deformation under high heating rate conditions. Similar to the pressure gap, the model was developed using uniaxial tensile tests under a constant load and temperature conditions. However, burst tests are transitory by nature, and the model appears inadequate in capturing the transitory behavior. Lastly, additional data under constant pressure conditions over a broad range of pressures would be invaluable to improving and validating the high-temperature creep model.

5. ACKNOWLEDGMENTS

This work was supported by the Department of Energy's (DOE) Nuclear Energy Advanced Modeling and Simulation (NEAMS) program. The authors would like to express their appreciation to Caleb Massey for providing detailed technical feedback. His feedback helped improve the technical content of the report.

6. REFERENCES

1. F. Erbacher and S. Leistikow, "Zircaloy Fuel Cladding Behavior in a Loss-of-Coolant Accident: A Review," in *Zirconium in the Nuclear Industry*, ed. R. Adamson and L. S. Van (West Conshohocken, PA: ASTM International 451–488 (1987).
2. M. Billone, Y. Yan, T. Burtseva, R. Daum, Cladding Embrittlement During Postulated Loss-of-Coolant Accidents, NUREG/CR-6967, U.S. NRC, Office of Nuclear Regulatory Research (2008).
3. Jinsu Kim, Jeong Whan Yoon, Hyochan Kim, Sung-Uk Lee, "Prediction of ballooning and burst for nuclear fuel cladding with anisotropic creep modeling during Loss of Coolant Accident (LOCA)," *Nuclear Engineering and Technology*, Volume 53, Issue 10 (2021). https://doi.org/10.1016/j.net.2021.04.020.
4. Gyeong-Ha Choi, Dong-Hyun Kim, Chang-Hwan Shin, Jae Yong Kim, Byoung Jae Kim, "In-situ deformation measurement of Zircaloy-4 cladding tube under various transient heating conditions

using optical image analysis," *Nuclear Engineering and Design* Volume 370 (2020). https://doi.org/10.1016/j.nucengdes.2020.110859.
5. Dong-Hyun Kim, Gyeong-Ha Choi, Hyochan Kim, Chan Lee, Sung-Uk Lee, Jong-Dae Hong, Hak-Sung Kim, "Measurement of Zircaloy-4 cladding tube deformation using a three-dimensional digital image correlation system with internal transient heating and pressurization," *Nuclear Engineering and Design*, Volume 363 (2020). https://doi.org/10.1016/j.nucengdes.2020.110662.
6. Hales, J. D., Williamson, R. L., Novascone, S. R., Pastore, G., Spencer, B. W., Stafford, D. S., Gamble, K. A., Perez, D. M., and Liu, W., "BISON Theory Manual: The Equations behind Nuclear Fuel Analysis," United States: N. p., 2016. Web. Doi:10.2172/1374503.
7. A. T. Donaldson and T. Healey, *Creep deformation of Westinghouse Zircaloy-4 fuel cladding tubes in alpha plus beta phase temperature range,* TRPD/B/056/N85, Central Electricity Generating Board, Berkely, Gloucestershire, UK (1984).
8. H. E. Rosinger, P. C. Bera, and W. R. Clendening, "Steady-state creep of Zircaloy-4 fuel cladding from 940 to 1873 K," *J. Nucl. Mater*., **82**:286–279 (1979).
9. N. Capps, Y. Yan, A. Raftery, Z. Burns, T. Smith, K. Terrani, K. Yueh, M. Bales, K. Linton, "Integral LOCA fragmentation test on high-burnup fuel," *Nucl. Eng. Des*. **367**, 110811, ISSN 0029-5493 (2020).
10. R.L Williamson, N.A. Capps, W. Liu, Y.R. Rashid, B.D. Wirth, "Multi-dimensional simulations of LWR fuel behavior in the BISON fuel performance code," *JOM* (2016). ISSN 1047–4838.
11. R. Williamson, J. Hales, S. Novascone, M. Tonks, D. Gaston, C. Permann, D. Andrs, R. Martineau, "Multidimensional multiphysics simulation of nuclear fuel behavior," *J. Nucl. Mater*. **423** 149–163 (2012).
12. R.L. Williamson, K.A. Gamble, D.M. Perez, S.R. Novascone, G. Pastore, R.J. Gardner, J.D. Hales, W. Liu, A. Mai, "Validating the BISON fuel performance code to integral LWR experiments," *Nucl. Eng. Des*. **301** 232–244 (2016). ISSN 0029-5493.
13. Permann, C. J., Gaston, D. R., Andrš, D., Carlsen, R. W., Kong, F., Lindsay, A. D., ... & Martineau, R. C., "MOOSE: Enabling massively parallel multiphysics simulation. SoftwareX, 11, 100430 (2020).
14. R.L. Williamson, K.A. Gamble, D.M. Perez, S.R. Novascone, G. Pastore, R.J. Gardner, J.D. Hales, W. Liu, A. Mai, "Validating the BISON fuel performance code to integral LWR experiments," *Nuclear Engineering and Design*, Volume 301, Pages 232–244, ISSN 0029-5493 (2016). https://doi.org/10.1016/j.nucengdes.2016.02.020.
15. Williamson, R. L., Pastore, G., Spencer, B. W., Hales, J. D., and Tverberg, T., "BISON Validation for LOCA and PCMI Behavior Using Measurements from the Halden Reactor Project," United States: N. p., 2017. Web.
16. Hales, J. D., Williamson, R. L., Novascone, S. R., Pastore, G., Spencer, B. W., Stafford, D. S., Gamble, K. A., Perez, D. M., and Liu, W., "BISON Theory Manual: The Equations behind Nuclear Fuel Analysis," United States: N. p., 2016. Web. Doi:10.2172/1374503.
17. S. YAGNIK, "Thermal conductivity recovery phenomenon in irradiated UO_2 and (U,Gd)O_2," *Proc. of Int. Top. Mtg. on LWR Fuel Performance*, Parkcity, Utah (2000).
18. M. LIPPENS and L. MERTENS, *High burnup UO_2 and (U,Gd)O_2 thermal diffusivity measurements and post-irradiation characterizations*, EPRI Report TR-106501 (1996).
19. LJ Siefken, EW Coryell, EA Harvego, and JK Hohorst, *SCDAP/RELAP5/MOD3.3 Code Manual: MATPRO–ALibrary of Materials Properties for Light-Water-Reactor Accident Analysis*, Technical Report NUREG/CR-6150, Vol.4, Rev.2, U.S. Nuclear Regulatory Commission (2001).
20. Laura P. Swiler, Richard L. Williamson, and Danielle M. Perez, "Calibration of a fuel relocation model in BISON," In *International Conference on Mathematics and Computational Methods Applied to Nuclear Science & Engineering*, Sun Valley, Idaho, May 5–9. American Nuclear Society (2013).

21. G. Pastore, L. Luzzi, V. Di Marcello, and P. Van Uffelen, "Physics-based modelling of fission gas swelling and release in UO_2 applied to integral fuel rod analysis," *Nuclear Engineering and Design*, 256:75–86 (2013).
22. K. Sakai, *The fuel creep test IFA-701: results after four irradiation cycles*, Technical Report HWR-1039, OECD Halden Reactor Project (2013).
23. K. Sakai, H. Hanakawa, and T. Tverberg, *Investigation of fission induced creep of UO2 and Cr-doped fuel in IFA-701*, Technical Report HWR-1006, OECD Halden Reactor Project (2011).
24. R. Szoke and T. Tverberg, *Update on in-pile results from the fuel creep test IFA-701*. Technical Report HWR-1092, OECD Halden Reactor Project (2014).
25. G. Pastore, L. Luzzi, V. Di Marcello, and P. Van Uffelen, "Physics-based modelling of fission gas swelling and release in UO_2 applied to integral fuel rod analysis," *Nuclear Engineering and Design*, **256**:75–86 (2013).
26. J. K. Fink and L. Leibowitz, "Thermal conductivity of zirconium," *Journal of Nuclear Materials*, **226**:44–50 (1995).
27. DG Franklin, "Zircaloy-4 cladding deformation during power reactor irradiation," in *Zirconium in the Nuclear Industry*, ASTM International (1982).
28. M. Limbäck and T. Andersson, "A Model for Analysis of the Effect of Final Annealing on the In- and Out-of-Reactor Creep Behavior of Zircaloy Cladding," in *Zirconium in the Nuclear Industry: Eleventh International Symposium*, ed. E. Bradley and G. Sabol (West Conshohocken, PA: ASTM International, 448–468 (1996).
29. F. J. Erbacher, H. J. Neitzel, H. Rosinger, H. Schmidt, and K. Wiehr, "Burst criterion of Zircaloy fuel claddings in a loss-of-coolant accident," in *Zirconium in the Nuclear Industry, Fifth Conference, ASTM STP 754, D.G. Franklin Ed.*, 271–283. American Society for Testing and Materials (1982).
30. N. E. Hoppe, "Engineering model for zircaloy creep and growth," in *Proceedings of the ANS-ENS International Topical Meeting on LWR Fuel Performance*, 157–172. Avignon, France, April 21–24 (1991).
31. N. Capps and R. Sweet, "Model for Determining Rupture Area in Zircaloy Cladding under LOCA Conditions," *Nuclear Engineering & Design*, under review (2022).
32. Tyler J. Gerczak, Chad M. Parish, Philip D. Edmondson, Charles A. Baldwin, Kurt A. Terrani, "Restructuring in high burnup UO_2 studied using modern electron microscopy," J*ournal of Nuclear Materials*, Volume 509 (2018). https://doi.org/10.1016/j.jnucmat.2018.05.077.
33. J. A. Turnbull, et al., "An Assessment of the Fuel Pulverization during LOCA-type Temperature Transients," *Nucl. Sci. and Eng*. **179**, 1–5 (2015).
34. V. Di Marcello, A. Schubert, J. van de Laar, and P. Van Uffelen. The TRANSURANUS mechanical model for large strain analysis. *Nuclear Engineering and Design*, 276:19–29, 2014